Future Changes in Biological Activity in the North Pacific due to Anthropogenic Forcing

David W. Pierce

Climate Research Division, Scripps Institution of Oceanography
La Jolla, California

18 June 2002

Submitted to *Climatic Change*

ABSTRACT

Many studies have examined the physical changes expected in the environment as a result of anthropogenic forcing. These physical changes will have an effect on ecosystems as well. In this study, a nitrogen-phytoplankton-zooplankton (NPZ) model is used to examine the effects of environmental changes on primary productivity in the North Pacific ocean. The physical variables considered are mixed layer temperature and depth, solar insolation, and large-scale upwelling. The changes in these fields by the 2090s are taken from a coupled ocean-atmosphere general circulation model forced by projected atmospheric CO_2 and sulfates, then applied to the NPZ biological model. The result is a 20-30% reduction in primary productivity in a belt of longitudes across the North Pacific. This happens because the region where spring blooms occur moves northwards in response to the anthropogenic changes. The region left behind (which had spring blooms in the 2000s, but does not in the 2090s) is less productive when averaged over a year. In other regions, productivity increases as warmer surface waters enable higher growth rates. Changes in mixed layer temperature and depth account for almost all the changes in productivity; model-predicted changes in surface insolation and large-scale upwelling have little impact.

1. Introduction

Many studies have used coupled climate models to look at the physical changes expected in the world due to anthropogenic forcing. However, changes in the physical environment can have effects on ecosystems as well. Alterations in ecosystems, in turn, can have impacts on people and society; for example, fish populations affect both food supplies and jobs. Therefore, it is important to examine the predicted effects of changes in the environment on ocean ecosystems.

Ecosystems are too complicated to model in a complete way, so the following approach was adopted for this work. First, a few physical variables of interest that might change due to anthropogenic forcing were selected. Then, the simplest ecosystem model that depended on those variables of interest was chosen and this model's response to the environmental changes was analyzed. The understanding gained this way can form the basis for examining more complicated biological models in the future.

The physical variables of interest were the following:

1. *Mixed layer depth*. Deeper mixed layers can mix up more nutrients from below, but also are darker (less light-driven production) near the bottom.

2. *Mixed layer temperature*. Warmer temperatures allow higher growth rates.

3. *Upwelling velocity*. Large-scale changes in the surface wind field can affect how much nutrient-rich deep water is upwelled from below.

4. *Solar insolation*. The amount of sunlight falling on the ocean's surface might change due to changes in cloudiness or sea ice coverage. This will directly affect the phytoplankton's light-driven production.

The predicted changes in physical variables were obtained from anthropogenically-forced runs generated by pilot accelerated climate prediction initiative (pilot-ACPI) program (Barnett et al. 2002). Although ACPI's focus was on hydrology in the western U.S., the global data set produced in that effort was appropriate for forcing the biological model described here. In the spirit of concentrating on ACPI's region of interest, attention here will be focused on the North Pacific. Important fisheries are located in the North Pacific (e.g., salmon) that have a substantial effect on the economy of the western states. Polovina et al. (1995) have previously examined natural climate variability in this region using a biological model similar to that employed here.

The rest of this paper is organized as follows. In section 2, the physical model used in the pilot-ACPI program is described. The biological model is described in section 3 and the equations are given in Appendix A. Section 4 shows the changes in physical environment that the physical model projects for the decade of the 2090s. The biological model's response to these changes over the North Pacific is shown in section 5. A more detailed analysis of the seasonal cycle at certain points of interest is given in section 6. The discussion in section 7 focusses on the key role of the effective growth rate in determining the biological model's response to the changing environment. Conclusions are given in section 8.

2. Physical Model Overview

The physical model used here is the Parallel Climate Model (PCM), version 1 (Washington et al. 2000). PCM is a state of the art, fully coupled ocean-atmosphere general circulation model (for more information see http://www.cgd.ucar.edu/pcm).

The atmospheric component of the PCM is the CCM3 atmospheric general circulation model developed at the National Center for Atmospheric Research (Kiehl et al. 1998), a spectral model used here at T42 resolution (equivalent to about 280 by 280 km grid spacing). CCM3 includes a land surface model that accounts for soil moisture and vegetation types, as well as a simplified runoff scheme. A hybrid sigma coordinate scheme with 18 layers is used in the vertical, which allows terrain-following coordinates near the surface but segues to pressure levels higher in the air column.

The ocean component of PCM is the Parallel Ocean Program (POP), developed at the Los Alamos National Laboratory (Smith et al. 1992, Dukowicz and Smith 1994), used here at a horizontal resolution of 384 by 288 gridpoints (roughly 2/3° resolution), with 32 vertical levels. The vertical levels are clustered near the surface to improve resolution of the important surface mixing processes. A displaced-pole grid is used in the northern hemisphere to eliminate the problem of convergence of the meridians in the Arctic Ocean.

A dynamic-thermodynamic sea-ice model based on Zhang and Hibler (1997) is included, with an elastic-viscous-plastic rheology for computational efficiency (Hunke and Dukowicz 1997). The ice model is formulated on its own grid, which has a total of 320 by 640 gridpoints. The grid only covers the polar regions, and points are distributed approximately equally between the northern and southern hemispheres (i.e., each hemisphere is covered by a grid of about 320x320 points), giving a physical grid spacing of roughly 27 km.

The PCM runs used here start in 1870 and end in 2099, using historical estimates of carbon dioxide and sulfates up until the present, and business-as-usual (BAU) projections of these quantities for future years. There are five ensemble members available for this work, but for the results shown here only one ensemble member was used, at it represents expected future change to first order without leading to problems with interpreting averages in the presence of non-linearities (i.e., the response to averaged forcing is not the same as the

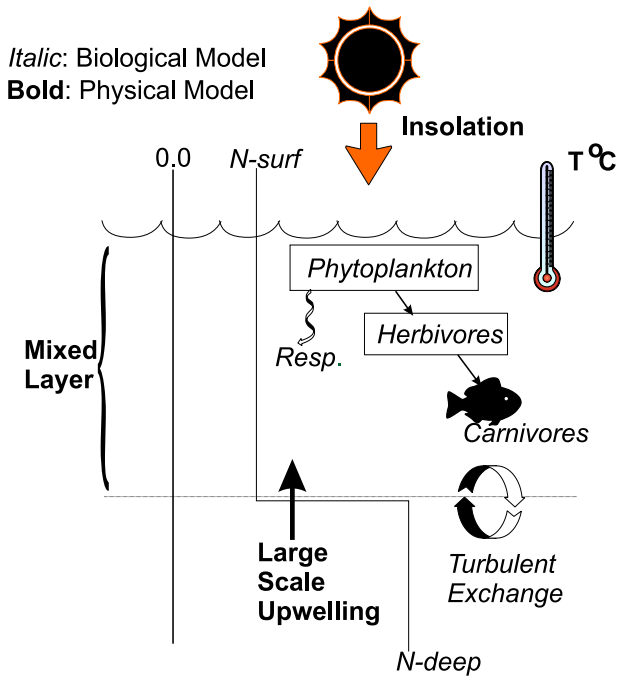

Figure 1: A schematic of the NPZ biological model. Forcing terms taken from the physical model are indicated in bold, while elements of the biological model are indicated in italic.

averaged response to individual forcing for non-linear processes). The results shown here compare the decade of the 2000s to the decade of the 2090s.

3. Biological Model Overview

The biological model includes nitrogen, phytoplankton, and herbivores (a so-called NPZ model, with Z referring to herbivorous zooplankton), and is based on the work of Evans and Parslow (1985; EP85 hereafter). The equations for the model are given in Appendix A, while a schematic overview is shown in Fig. 1. There is a well-mixed upper layer of thickness M and temperature T, both of which are specified from the physical model (PCM). The mixed layer contains phytoplankton, which are eaten by herbivores, which in turn are eaten by carnivores. The phytoplankton locally release nutrients back into the mixed layer via respiration. At the base of the mixed layer, both local turbulent exchange and large-scale upwelling mix nutrients up from below.

The separation into the two mixing components (large-scale upwelling and local turbulent exchange) is a departure from the way vertical mixing was parameterized in EP85, which had only a fixed vertical exchange taking into account both these effects. Here, the large-scale upwelling is taken from the physical model, with a constant value used for the local turbulent exchange. Ideally, the local turbulent mixing would have been taken from the physical model as

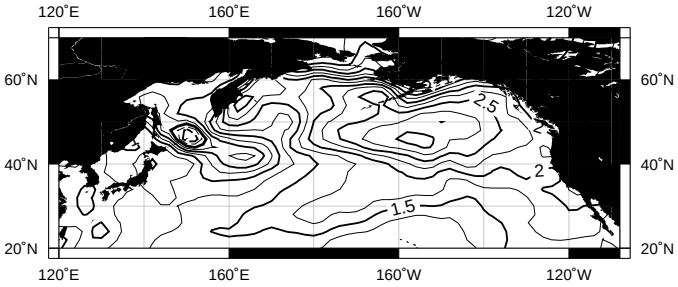

Figure 2: Difference in mixed layer temperature (C) between the decade of the 2090s and the decade of the 2000s, during the growing season (MAMJ). Contour interval is 0.25 C.

well, however, these terms were not saved in the physical model runs. Inclusion of the large-scale upwelling allows the biological model to adjust to large-scale changes in the wind field that drive different patterns of Ekman upwelling or downwelling. Upwelling carries more nutrients up into the mixed layer, while downwelling reduces the vertical flux of nutrients.

Solar forcing is taken from the physical model. This allows changes in the light-driven production if, for example, the physical model predicts systematic differences in cloudiness arising from anthropogenic forcing.

Following Sarmiento et al. (1993) and Polovina et al. (1995), the maximum growth rate is taken to be a function of mixed layer temperature as follows: $P_{\max} = 0.6(1.066)^T$, where T is the mixed layer temperature in degrees C.

Biological model parameters are taken from EP85 with the few exceptions noted in Appendix A, and are appropriate to the extratropical region. Accordingly, we will focus on the area in the Pacific between 20°N and 70°N.

4. Physical forcing

The changes in the four forcing variables (mixed layer temperature and depth, solar insolation, and upwelling velocity) will now be shown for the decade of the 2090s versus the 2000s. Because changes in the physical environment are most important during the phytoplankton growing season, results will be shown averaged over the time period March-April-May-June (MAMJ).

a. Mixed layer temperature

Figure 2 shows the mixed layer temperature in the physical model for the growing season during the decade of the 2090s versus 2000s. Mixed layer temperatures are considerably warmer (by about 1.5-3.0°C) during the 2090s; the warming is more pronounced in the more northerly part of the region. Since the maximum growth rate depends monotonically on temperature, this warming means that growth rates in the 2090s will generally be higher than in the 2000s.

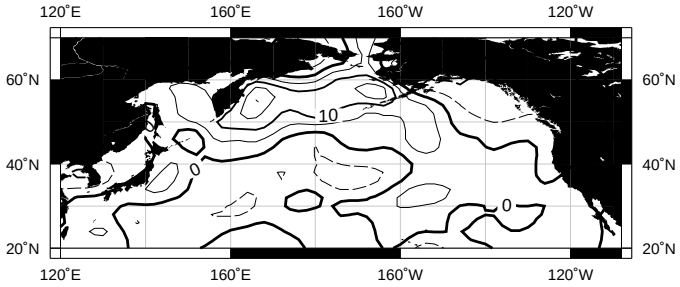

Figure 3: Difference in surface solar insolation (W m^{-2}) between the decade of the 2090s and the decade of the 2000s, during the growing season (MAMJ). Contour interval is 5 W m^{-2}. Negative contours are dashed.

PCM's climate sensitivity is about 1.5° C to a doubling of atmospheric CO_2 (Washington et al. 2000), which is on the low end of the frequently accepted range of 1.5° C to 4.5° C for various coupled climate models (IPCC 2001).

b. Solar forcing

Figure 3 shows the surface solar insolation in the physical model for the growing season during the decade of the 2090s versus 2000s. There is a decrease in seasonal (highly reflective) sea ice in the far North Pacific that results in an increase in net surface solar insolation of about 10-15 W/m^2. This increase in raw solar insolation is translated to an increase in photosynthetically active radiation (PAR) as in EP85.

c. Upwelling velocity

Figure 4 shows the large-scale upwelling calculated by the model. The sense of the vertical velocity is such that Ekman suction (upwelling) occurs over the subpolar gyre, while Ekman pumping (downwelling) is found over the subtropical gyre. Larger values can be seen along the coast (for example, the west coast of North America), which drives increased productivity in those regions. The difference between the vertical velocity in the 2000s and 2090s is small (Fig. 4, bottom panel), and it will be seen later that this change has little effect on the biology.

d. Mixed layer depth

Figure 5 shows the ratio of the mixed layer depth in the 2090s to the 2000s (the ratio is shown instead of the difference because of the large dynamic range). Over the majority of the Pacific north of 20° N, the ratio is less than one, indicating that mixed layer depths are thinner in the 2090s. The exception is a region near the Bering Sea, where depths are slightly greater in the 2090s. The depth of the mixed layer can have two contrasting effects on the biology; in light limited regions (generally the higher latitudes), a deeper mixed layer results in less light, with a consequent decrease in phytoplankton growth rate. In nutrient limited regions (gener-

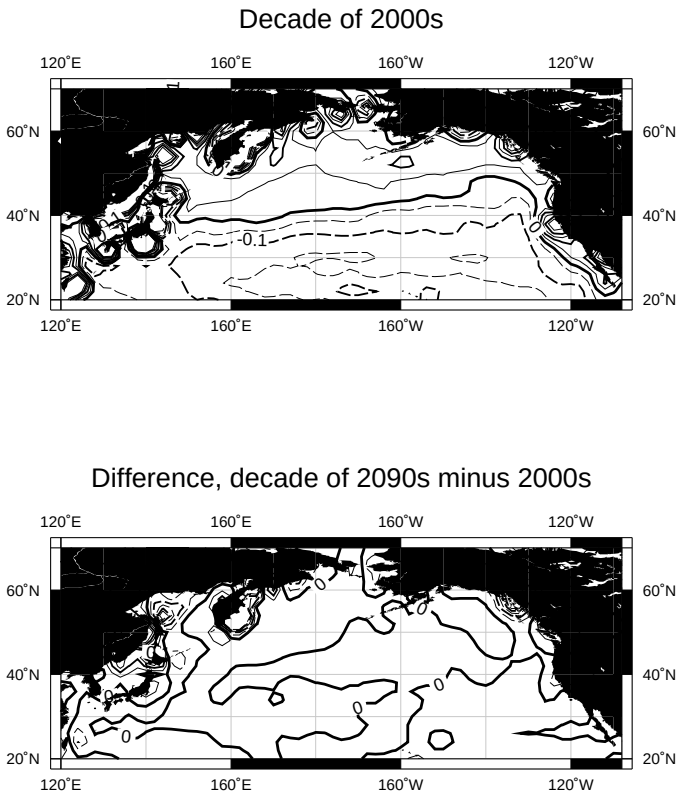

Figure 4: Upwelling velocity (m/day) at the base of the mixed layer. Top: for the decade of the 2000s. Bottom: difference between decade of the 2090s and 2000s. All values are averaged over the growing season (MAMJ). Contour interval is 0.05.

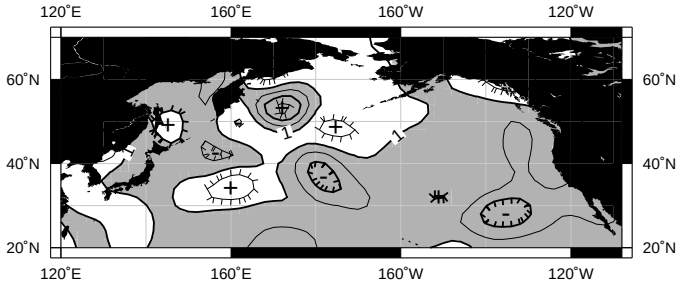

Figure 5: Ratio of the mixed layer depth in the 2090s to that in the 2000s. All values are averaged over the growing season (MAMJ). Contour interval is 0.05. Values less than 1 (indicating shallower mixed layers in the 2090s) are shaded.

ally the lower latitudes), a deeper mixed layer increases the flux of nutrients from below, with an attendant increase in phytoplankton growth rates.

5. Biological model response

The response of the biological model to the environmental changes outlined above will now be shown. All values and figures in this section are averaged over the growing season (March-April-May-June); annual cycles at various locations are presented in section 6.

Figure 6 shows the growing season phytoplankton concentration in the NPZ model. There is a arc of high values along the continental coasts, with generally higher values in the subpolar gyre (where the upwelling occurs) than in the subtropical gyre (downwelling). Values range from 0.27 mmN m^{-3} in the central subtropical gyre to values of about 2.0 mmN m^{-3} near the coasts.

The bottom panel of Fig. 6 shows the ratio of phytoplankton concentration in the 2090s to the 2000s. Again, the ratio is used because of the large dynamic range involved. The main change is a decrease in concentrations in the subpolar gyre on the order of 20-40%. A predicted reduction in yearly averaged phytoplankton concentrations in the subpolar North Pacific is one of the primary results of the NPZ model; the reason for this decrease will be explained once all the changes in the biological model have been illustrated.

Figure 7 shows observed phytoplankton pigment (chlorophyll) concentration (mg Chl m^{-3}) from the coastal zone color scanner (CZCS)[1]. In comparison with the observations, the model does not capture the extent to which the phytoplankton concentrations are enhanced near the coasts, especially along the west coast of North America. This is likely due to the biological model's use of a single, constant vertical turbulent mixing parameter (equivalent to 0.3 cm^2 s^{-1}; see Appendix A) that is appropriate to the open ocean. Enhanced mixing near the coasts, especially over the continental shelves, would increase phytoplankton concentrations in those regions, an effect that is currently ignored. This can be seen particularly along the west coast of North America. Note that the actual numbers in Fig. 7 cannot be directly compared to those in Fig. 6 because the former are pigment concentrations while the latter are nitrogen concentrations. An approximate conversion using a Redfield ratio of 106C:16N:1P, and assuming that the carbon-to-chlorophyll ratio is 30-50 mg carbon per mg chlorophyll, suggests that the model's phytoplankton concentrations are too large. This could be ameliorated by tuning the biological model parameters, however this was not done since the purpose of this work is to *understand the reasons* for changes in the ocean ecosystem between the 2000s and the 2090s, rather than to *tune the model* to reproduce current conditions as closely as possible. Such tuning would have no effect on

[1]Data downloaded from http://daac.gsfc.nasa.gov/data/dataset/CZCS

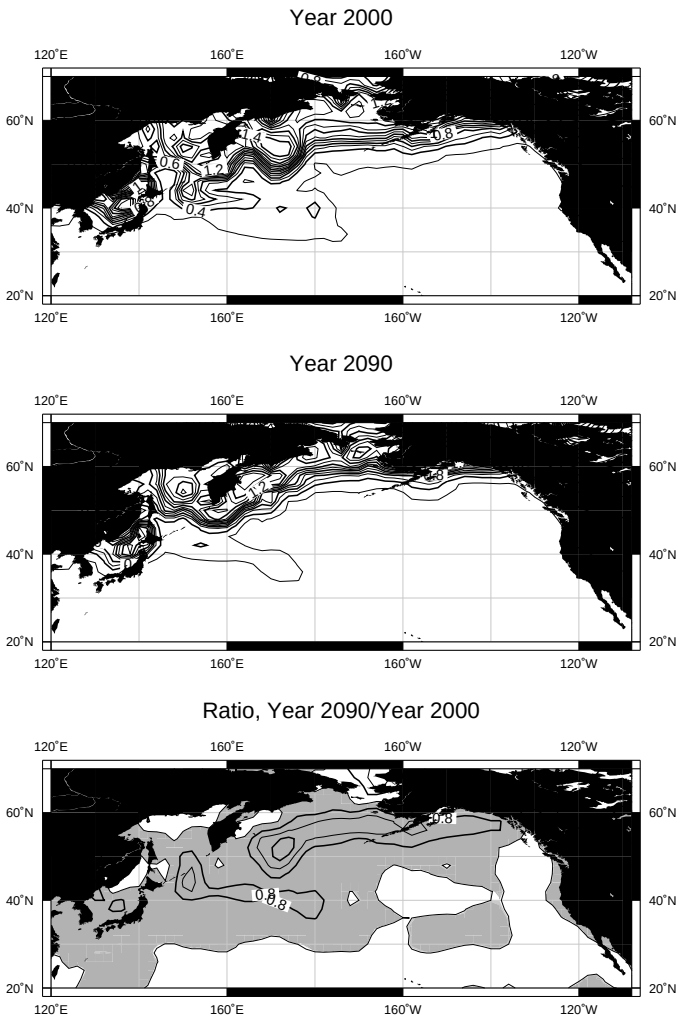

Figure 6: Growing season (MAMJ) phytoplankton concentrations (mmN m^{-3}) from the biological model. Top: decade of the 2000s. Middle: the 2090s. Bottom: Ratio of the 2090s to the 2000s. Values less than one (indicating reduced concentrations in the later decade) are shaded. Contour interval for all panels is 0.1.

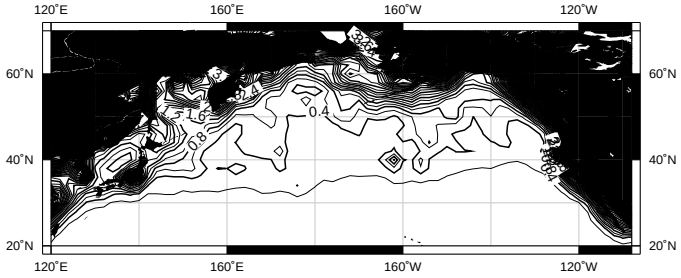

Figure 7: Phytoplankton pigment concentrations (mg/m^3) from the coastal zone color scanner satellite for spring (MAMJ).

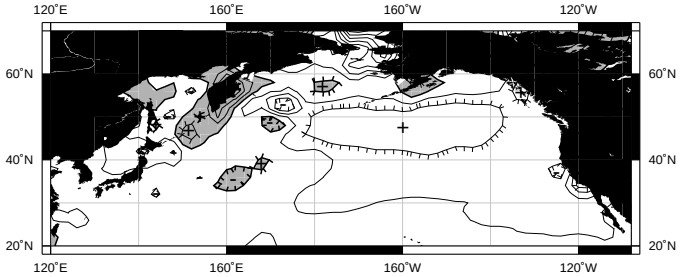

Figure 8: The ratio of herbivore concentration in the growing season averaged over the decade of the 2090s over the decade of the 2000s. Values less than one (indicating reduced concentrations in the 2090s) are shaded. Contour interval is 0.1.

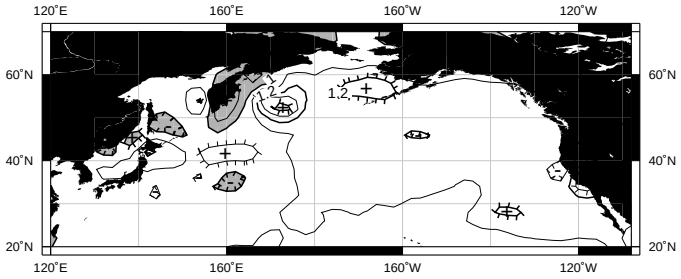

Figure 9: The ratio of growth rate (day^{-1}) during the growing season, averaged over the decade of the 2090s over the decade of the 2000s. Values less than one (indicating lower growth rates in the 2090s) are shaded. Contour interval is 0.1.

the conclusions presented in section 8.

Figure 8 shows the ratio of the herbivores in the 2090s to that in the 2000s. The later decade has herbivore concentrations in the subpolar gyre that are 20-30% higher than in the earlier decade. This tendency can be understood from the equilibrium solutions (Appendix A; in particular, Eq. 12), where it is shown that the equilibrium herbivore concentration is directly proportional to the growth rate. (The equilibrium solutions are the phytoplankton, nitrogen, and herbivore concentrations that would be seen if the biological system responded instantaneously to the changing physical forcing. Departures from equilibrium conditions can lead to overgrazing and consequently low values of phytoplankton concentrations, or to unchecked population explosions that lead to spring blooms.)

The previous two illustrations were in terms of phytoplankton and herbivore concentrations. However, a more relevant quantity to the food chain is the primary productivity, R, defined as $R = PM\alpha$, where P is the phytoplankton concentration, M is the mixed layer depth, and α is the growth rate. The ratio of growth rates in the 2090s to the 2000s is shown in Fig. 9. Growth rates are almost univer-

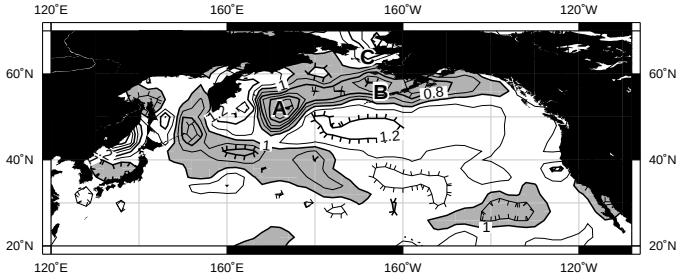

Figure 10: The ratio of primary productivity (mmN m^{-2} day^{-1}) during the growing season, for the decade of the 2090s over the decade of the 2000s. Values less than one (indicating reduced productivity in the latter period) are shaded. Contour interval is 0.1.

sally higher in the later decade. The increase in growth rate is driven primarily by the warmer mixed layer temperatures (Fig. 2), since the maximum growth rate is taken to be a function of mixed layer temperatures. The effect of shallower mixed layers (Fig. 5) can also be seen in those places where the shallowing is strong, and hence the mixed layer is better lit.

The ratio of primary productivity averaged over the growing season in the 2090s to the 2000s is shown in Fig. 10. The net result of the changes in phytoplankton concentrations, mixed layer depth, and growth rate is a reduction in productivity by 20-40% in the 2090s in the region of the subpolar gyre. In the Bering sea, by contrast, productivity increases by a similar amount.

6. Analysis

The biological model suggests that by 2090, phytoplankton concentrations and primary productivity will decrease in the subpolar North Pacific and increase in the Bering sea. What physical forcings are responsible for the biological response in these regions, and why does the biological model respond with pronounced regional differences? The answers to these questions will allow an *understanding* of how the biology may respond to future environmental changes, rather than simply obtaining an *answer* from the biological model results. This allows evaluation of the model's response in a larger picture of uncertainty in predictions of future environmental changes.

In this analysis we will make use of the three points shown in Fig. 10: point A in the western North Pacific (170°E, 49°N); point B in the central North Pacific (165°W, 51°N); and point C in the Bering sea (167°W, 62°N). These points were selected because they exemplify the biological model's response in three dissimilar regions. Points were used, rather than averaging over regions of interest, because the nonlinear nature of the biological model (Appendix A) means that the average biological response over a box is not the

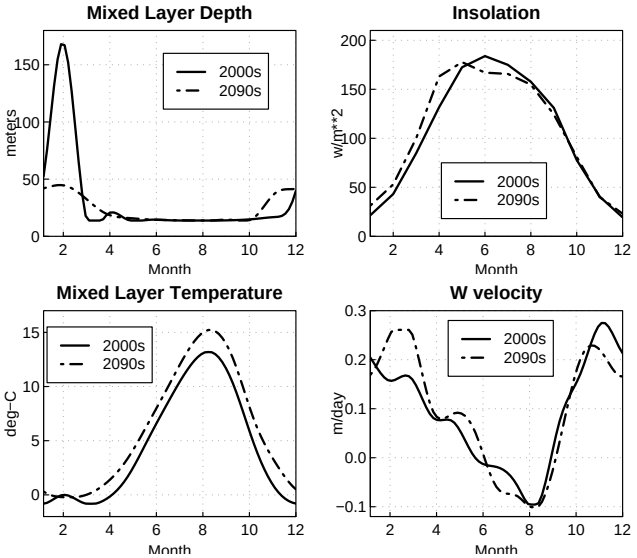

Figure 11: Components of the physical forcing for the decade of the 2000s (solid line) and 2090s (dashed line), at point A in the western North Pacific shown in Fig. 10.

same as the response of the model to the average forcing over the box. Analysis at points avoids this problem, allowing a cleaner interpretation of the results. These results will then be extended to the entire North Pacific in section 7.

a. Western North Pacific

The components of the physical forcing at point A, in the western North Pacific, are shown in Fig. 11. The main differences between the 2000s and the 2090s is a strong reduction in winter mixed layer depth associated with the capping of the water column by the warmer water. Changes in upwelling and solar insolation are small by comparison.

The biological model response at point A is shown in Fig. 12. Concentrating for the moment on the contrast between the decade of the 2000s (thick solid line) and the 2090s (thick dashed line), it can be seen that the phytoplankton concentration (Fig. 12a) undergoes a substantial springtime enhancement in this region in the 2000s, but is nearly constant in the 2090s. This change is accompanied by an increase in herbivore concentration and effective growth rate.

To determine the physical forcings responsible for the biological response, four permutation test runs were performed. The standard run for the decade of the 2000s used the four forcing components (mixed layer temperature, mixed layer depth, large-scale upwelling, and solar insolation) from physical model with values averaged over the 2000s, and likewise for the 2090s run. For the permutation runs, *one*

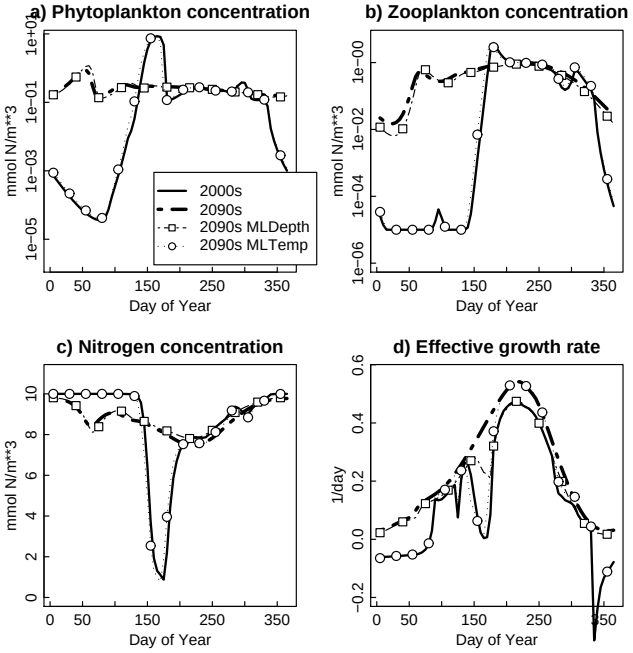

Figure 12: Annual cycle of phytoplankton, herbivore, and nitrogen concentrations (mmN m^{-3}), and effective growth rate (day^{-1}), from the biological model at point A in the western North Pacific. The physical forcing applied to the various runs is indicated in the legend.

of the four forcing components was taken from the 2090s, while the rest were taken from the 2000s. This allows us to determine how the four forcings individually influence the changes in biology seen in the 2090s. (The final response will not be the sum of the four individual influences because of non-linearities.)

The results of the permutation runs at point A are also shown in Fig. 12. For clarity, the annual cycles for the cases with permuted upwelling and solar forcing are omitted; it was found that changes in these forcings had little effect on the biological cycle. In panel 12a, comparing the results with *only* mixed layer temperatures taken from the 2090s (circles) to that with only mixed layer depths taken from the 2090s (squares), it can be seen that most of the change in phytoplankton and herbivore concentrations seen in the 2090s arise from changes in the mixed layer depth alone.

This can be understood from the results in EP85, which demonstrate that rapid specific changes in the growth rate enable the kind of spring bloom seen in the 2000s but not the 2090s. The effective growth rate, γ, is shown in Fig. 12d; defined in Appendix A (Eq. 6), γ takes into account the phytoplankton growth rate, α, but is modified by losses due to respiration and vertical mixing. In this location, γ becomes negative in the dim midwinter months during the 2000s, as the phytoplankton concentration has negative tendencies due to respiration and the rapidly deepening mixed layer that exceed α. With the sudden shallowing of the mixed layer in the winter, γ becomes positive; the transition of γ through zero guarantees that the specific change in growth rate, $(1/\gamma)d\gamma/dt$, becomes large, leading inexorably to a spring bloom. This behavior does not occur in the 2090s, when the capping of the column by warmer surface water prevents γ from ever becoming negative (Fig. 12d, squares). In other words, the phytoplankton in the 2090s are held closer to the surface in winter, where there is more light-driven production, and are not subject to dilution by a rapid increase in mixed layer depth. Both these keep the effective growth rate positive even in midwinter, preventing the specific growth rate from becoming large enough to trigger a bloom.

In summary, the biological model suggests that productivity in the western North Pacific will decrease because increasing stratification of the water column prevents a rapid late winter shallowing of the mixed layer, thereby eliminating the circumstances that formerly led to a spring bloom in the region.

b. Central North Pacific

The components of the physical forcing at point B, in the central North Pacific, are shown in Fig. 13. The region is characterized by a warming of mixed layer temperatures by almost 3°C in the 2090s, along with modest changes in mixed layer depth and small changes in insolation and upwelling.

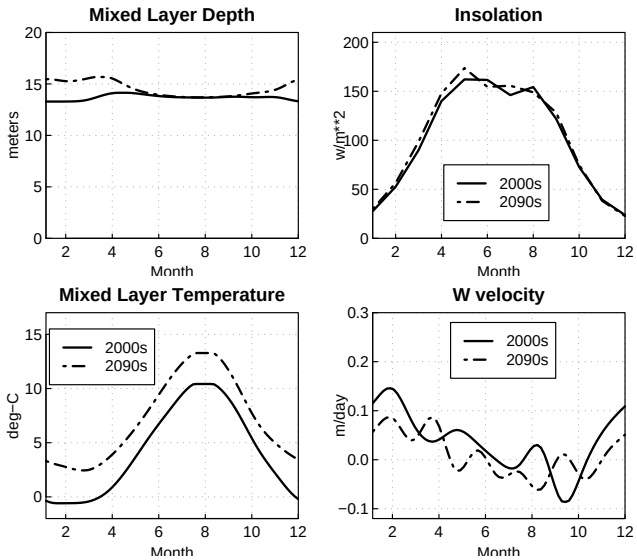

Figure 13: Components of the physical forcing for the decade of the 2000s (solid line) and 2090s (dashed line), at point B in the central North Pacific shown in Fig. 10.

The biological response in the central North Pacific is shown in Fig. 14. There is again a distinct decrease in the amplitude of the spring bloom going from the 2000s to the 2090s. In this case, the permutation runs show that the change in mixed layer depth and temperature each separately have about the same effect, and it is the combination of the two that accomplishes the reduction in phytoplankton concentrations.

The fact that warmer mixed layer temperatures reduce the phytoplankton concentration is, on the surface, somewhat counter-intuitive. *Warmer* mixed layer temperatures are associated with *increases* in the growth rate but a *decrease* in the phytoplankton concentration. This can again be understood by considering the effective growth rate (γ), Fig. 14d. In the 2000s, γ becomes negative in midwinter (around day 345). As in the western North Pacific, γ increasing through zero leads inevitably to a spring bloom. However, the warmer surface temperatures and shallower mixed layer depths in the 2090s boost γ to the point where it never quite becomes negative (Fig. 14d, thick dashed line). The size of the spring bloom is thus mitigated, and average phytoplankton concentrations decrease.

The reason the temperature-driven increase in γ had little effect in the western North Pacific, while it is important here, is because γ contains contributions from both the mixed layer depth and temperature (Eq. 6). In the west-

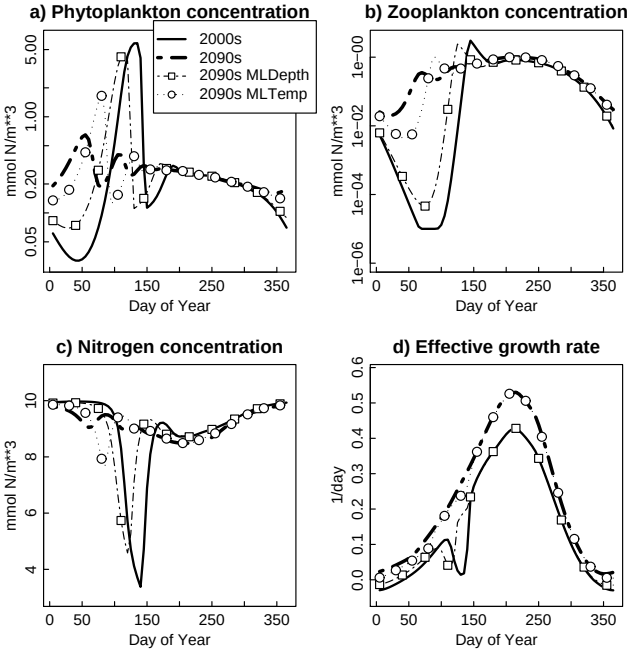

Figure 14: Annual cycle of phytoplankton, herbivore, and nitrogen concentrations (mmN m^{-3}), and effective growth rate (day^{-1}), from the biological model at point B in the western North Pacific. The physical forcing applied to the various runs is indicated in the legend.

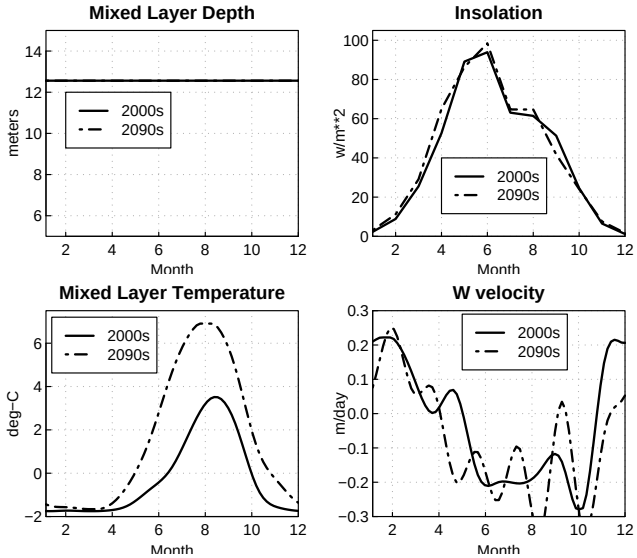

Figure 15: Components of the physical forcing for the decade of the 2000s (solid line) and 2090s (dashed line), at point C in the central North Pacific shown in Fig. 10.

ern North Pacific, the large changes in mixed layer depth overwhelm the changes due to temperature. In the central North Pacific, where the change in mixed layer temperature is about the same as in the western North Pacific but the changes in mixed layer depth are much more modest, both effects are important.

c. Bering Sea

The components of the physical forcing at point C, in the Bering Sea, are shown in Fig. 15. The strong halocline in this region prevents any discernible change in mixed layer depth between the 2000s and 2090s. Insolation and vertical velocity changes are likewise small. The main difference in this region is an increase in mixed layer temperatures during the summer months, after the sea ice has retreated.

The biological response in the Bering Sea is shown in Fig. 16. The phytoplankton bloom comes slightly earlier in the year during the 2090s, a consequence of the earlier mixed layer warming. The overall magnitude and evolution of the phytoplankton concentrations are otherwise similar between the two time periods. This is because the transition of γ through zero is almost the same in all cases (Fig. 16d). This, in turn, is because the physical factors that affect γ are little changed between the two decades. In particular, the transition of γ through zero occurs early in the year, when the mixed layer temperature is the same. Consequently, the increase in productivity seen in the region (Fig. 10) is due to

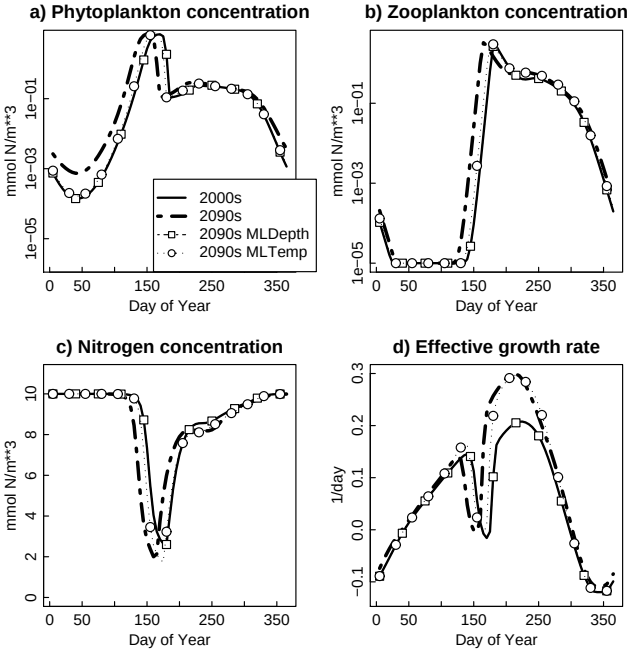

Figure 16: Annual cycle of phytoplankton (top) and herbivore (bottom) concentrations (mmN m^{-3}) from the biological model at point C in the central North Pacific. The physical forcing applied to the various runs is indicated in the legend.

summer increases in the growth rate (Fig. 16d) forced by the warmer mixed layer temperatures, rather than by changes in phytoplankton concentration (as was found in the western and central North Pacific).

7. Discussion

The results in the previous section illustrate the importance of $\gamma_{\min}$, the yearly minimum value of the effective growth rate (c.f. Sverdrup's 1953 critical depth theory). Where $\gamma_{\min}$ drops below zero in midwinter, the subsequent transition of γ through zero in the spring leads to large values of the specific effective growth rate $(1/\gamma)d\gamma/dt$, and consequently to a spring bloom. Where $\gamma_{\min}$ never becomes negative, the specific effective growth rate generally stays large enough to prevent a bloom, and phytoplankton concentrations tend to be near their equilibrium values at all times.

This dependence on $\gamma_{\min}$ suggests partitioning the North Pacific into three regions based on the following criteria:

1. $\gamma_{\min} > 0$ in both the 2000s and 2090s. In these locations, spring blooms tend not to occur, and phytoplankton concentrations are little different between the 2000s and 2090s. The main change in primary productivity in the 2090s therefore arises from changes in the phytoplankton growth rate α, which increases everywhere due to the mixed layer warming. In these regions modest increases in productivity are expected.

2. $\gamma_{\min} < 0$ in both the 2000s and 2090s. In these locations, spring blooms occur in both time periods. In lieu of significant changes in the spring bloom, future primary productivity is again most affected by effect of warmer surface waters on α. Therefore, primary productivity will tend to increase in these regions.

3. $\gamma_{\min} < 0$ in the 2000s, but > 0 in the 2090s. In these regions, the physical forcings are such that a bloom is seen in the 2000s but not in the later period. The increase in $\gamma_{\min}$ in the 2090s can be accomplished by either greater stratification leading to decreased winter mixing (as seen at point A, in the western North Pacific; section 6a) or by warmer mixed layer temperatures acting together with modest changes in mixed layer depths (point B, in the central North Pacific; section 6b). In these locations, the removal of the spring bloom results in decreased primary productivity, sometimes significantly, in the 2090s.

Figure 17 shows these three regions in the model. In the subtropics, $\gamma_{\min}$ is always positive (no shading), and there is no spring bloom now or in the future. North of about 55°N, $\gamma_{\min}$ is always negative (stipple), and spring blooms are found. The main effect of anthropogenic forcing is to push the boundary of the region where spring blooms are

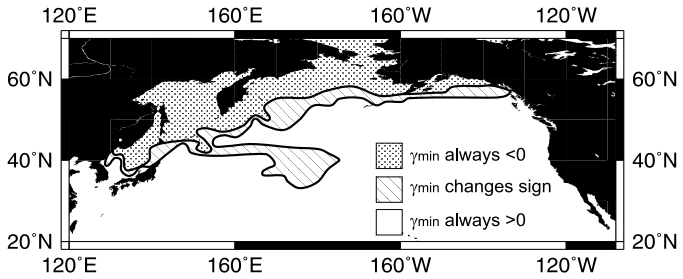

Figure 17: Regions where $\gamma_{\min}$ is negative in both the 2000s and 2090s (stipple), where $\gamma_{\min}$ is positive in both time periods (no shading); and where $\gamma_{\min}$ is negative in the 2000s but positive in the 2090s (crosshatch).

found to the north. This is because in the south, more constant daylight and warmer water temperatures keep the effective growth rate positive all year; in the north, the cold waters and weak sunlight in the winter enable the effective growth rate to drop below zero. There is necessarily a transition zone between the northern and southern regimes; and since the main effects of anthropogenic forcing relevant for the biology (warmer mixed layer temperatures and shallower mixed layer depths) both act in the direction of increasing $\gamma_{\min}$, the southern regime inevitably extends northwards. The simple biology of the NPZ model has a tendency to over-predict regions of spring bloom, for example in the eastern North Pacific, where processes not considered here might come into play (e.g., iron limitation (Martin et al. 1990), changes in zooplankton grazing (Frost 1991), or deep mixing (Mitchell et al. 1991); see also Obata et al. (1996)).

The conclusion that the region of spring phytoplankton blooms moves northward under anthropogenic warming is a robust prediction of the physical/biological model studied here. Different physical forcings (perhaps obtained from different coupled ocean-atmosphere models), or different parameters used in the biological model, will have the effect of shifting the particular latitudes where the regimes fall, but not in changing the behavior that anthropogenic forcing moves the spring bloom region northward. The only aspect of the physical forcing this conclusion depends on is that the warming signal in mixed layer temperature is monotonic over the region.

Regions that lose their ability to support spring blooms will have less primary productivity when averaged over the year. Elsewhere, the temperature-driven increase in growth rates will generally mean a higher primary productivity. In those regions that maintain their spring bloom (the far north), leading to large phytoplankton concentrations for a time, the absolute increase in primary productivity will be larger than in regions that are always near equilibrium phytoplankton concentrations (the region south of 50°N).

Although the results presented here are robust to details of the of the physical forcing, different biological systems than modeled here might behave differently. For example, in the real world, shifting distributions of species (each with their own way of reacting to the environment) might compensate for the changing environmental conditions. This question will need to be addressed by more elaborate biological models. In such a case, the results from the simple NPZ model studied here should provide a framework for understanding the more complete (and, presumably, more complicated) results.

8. Conclusions

Anthropogenic forcing can be expected to have an effect on ecosystems that respond to changes in the the physical environment. One example is the ocean ecosystem, where phytoplankton concentrations depend on water temperature, sunlight, mixed layer depth, and the upwelling of nutrients from below. This study has used the environmental predictions of a coupled ocean-atmosphere general circulation model run to the 2090s to force a NPZ (nitrogen-phytoplankton-zooplankton) biological model of the North Pacific. The physical variables considered were mixed layer temperature, mixed layer depth, surface solar insolation, and large-scale upwelling and downwelling.

It was found that primary productivity decreases in a belt of longitudes across the central North Pacific, while increasing in the Bering Sea and subtropical Pacific. This behavior can be understood by considering the phytoplankton's effective growth rate γ, which is the growth rate modified to take into account losses due to respiration and vertical mixing. North of about 50°N, γ becomes negative in the dim midwinter months; in the south, it is always positive. Large changes in the specific effective growth rate $(1/\gamma)d\gamma/dt$ lead to spring blooms, so in places with negative midwinter values of γ, spring blooms occur after γ transitions through zero.

The primary effects of the anthropogenic forcing are to warm the mixed layer and (more regionally) decrease mixed layer depths. Both tend to increase midwinter values of γ. This moves the region where spring blooms are possible farther to the north. The loss of spring blooms in the belt of longitudes left behind leads to lower primary productivity in that region when averaged over a year. In regions where the spring bloom (or lack thereof) does not change in the 2090s, productivity increases due to the higher growth rate.

The main conclusion of this work – that the region of spring blooms moves northwards due to anthropogenic forcing, leaving behind a lower-productivity region – is robust to details of the physical forcing used. Environmental changes from a different coupled ocean-atmosphere model would likely have given a similar result (although the exact latitude of the regions might well be different) as long as the

mixed layer warming is monotonic over the region. Changing the parameters for the biological model would similarly not change this conclusion, but rather would influence the exact latitudes involved. It should be kept in mind, however, that this conclusion might be modified by taking into account biological processes neglected in the simple NPZ model. For instance, were other species with different metabolic attributes or sensitivities to the environment included, the biology might respond by shifting the proportion of species instead. Consideration of such issues awaits results from more complex biological models.

9. Acknowledgments

The author would like to thank Douglas Nielson and Tim Barnett of SIO for helpful discussions. This work was supported by the Department of Energy under grant DE-FG03-98ER62505. The computations for the pilot-ACPI project were carried out under the auspices of the National Partnership for Advanced Computer Infrastructure (NPACI) at the San Diego Supercomputer center, with the help of Peter Arzberger and Giridhar Chukkpalli, and at the Oak Ridge National Laboratory, with the help of John Drake. These contributions are gratefully acknowledged.

Appendix A: Biological Model Equations

The biological model used here is similar to that described in EP85, with only a minor difference due to the splitting of the vertical mixing term into two components, large-scale upwelling and local turbulent mixing. The equations will be shown here for completeness and because the equilibrium model equations (also derived below) are based on the entire biological model, rather than on a reduced form of the model as was done in EP85.

The model is formulated in terms of the mixed layer depth, M, dissolved nitrogen concentration, N, and the concentration of nitrogen held in the phytoplankton (P) and herbivores (H). The time evolution of these quantities is given by:

$$\dot{M} = \zeta(t) \quad (1)$$

$$\dot{N} = -\gamma P + \mu(N_o - N - P) \quad (2)$$

$$\dot{P} = \gamma P - zH \quad (3)$$

$$\dot{H} = (fz - g - \frac{\zeta(t)}{M})H \quad (4)$$

The rate of mixed layer deepening, $\zeta(t)$, is taken from the physical model.

The vertical mixing term, μ, is given by:

$$\mu = \frac{m_e + m_t + \zeta^+(t)}{M} \quad (5)$$

where m_e is the large-scale upwelling or downwelling driven by Ekman processes (values taken from the physical model), m_t is a local turbulent exchange at the base of the mixed layer, and $\zeta^+(t) = \max(\zeta(t), 0)$ is the entrainment rate. The vertical mixing term in the herbivore equation is unlike that in the other equations (using ζ instead of ζ^+) because herbivores are assumed able to move up in the water column during times of detrainment. The *effective growth rate* term, γ, is given by:

$$\gamma = \frac{\alpha(t, M, P)N}{j + N} - r - \mu \quad (6)$$

It takes into account the phytoplankton growth rate, α, as well as losses to respiration (r) and vertical mixing (μ). Because γ is the dynamically important variable, not α, most of our analysis is done in terms of γ.

The term describing grazing of phytoplankton by herbivores, z, is given by:

$$z = \frac{c(P - P_0)}{K + P - P_0} \quad (7)$$

The meaning and values taken for the other parameters is the same as in EP85 (their table 1), and so are not repeated here, with the following exceptions. The local turbulent exchange, m_t, is taken to be 0.88 m day^{-1}; this value is equivalent to the amount exchanged in one day at the base of a vertical distribution with an initial step-function, given a large-scale vertical diffusivity of 0.3 cm^2 sec^{-1}. The attenuation of light due to water is taken to be 0.04, and the attenuation due to self-shading by the phytoplankton is taken to be 0.06; these values are taken from the subarctic Pacific experiment of EP85.

a. Equilibrium solutions

The equilibrium solutions to the model equations are obtained by setting the time derivatives to zero. The equilibrium phytoplankton concentration is:

$$P^* = P_o + \frac{K}{\phi - 1} \quad (8)$$

where $\phi = fc/(g - \zeta/M)$ represents a net grazing efficiency of the phytoplankton by the herbivores, and is the ratio of the nitrogen input to the herbivores by grazing to the nitrogen lost from the herbivores to carnivores or vertical mixing. For the values used here, $\phi \sim 7$. Thus, roughly speaking, $P^* \sim P_o + K/6 \sim 0.27$. This is a direct function of the grazing threshold P_o, and modified by a term inversely proportional to the net grazing efficiency. If the herbivore's grazing efficiency (f) or rate (c) decreases, ϕ decreases and there are more phytoplankton in equilibrium (P^* increases). If the loss of herbivores to carnivores (g) increases, then ϕ decreases and again the equilibrium phytoplankton concentration increases.

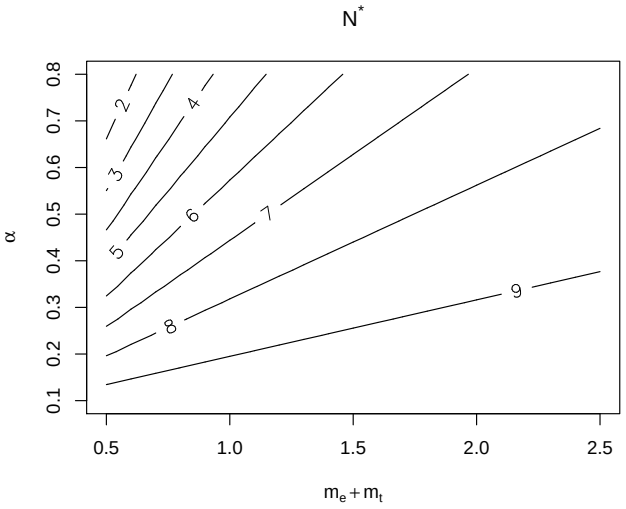

Figure 18: Equilibrium nitrogen concentration (mmN m^{-3}) as a function of total vertical mixing ($m_e + m_t$; m day^{-1}) and growth rate (α; day^{-1}).

The equilibrium nitrogen concentration is the solution to a quadratic equation, $(-b + (b^2 - 4ac)^{1/2})/2a$, where

$$a = 1 \quad (9)$$

$$b = (\alpha - r)P^*/\mu + j - N_o \quad (10)$$

$$c = -j(rP^*/\mu + N_o) \quad (11)$$

Although the solution to this is algebraically complicated, over a reasonable range of parameters the strongest dependence is on α, N_o, and the vertical mixing ($m_e + m_t$). The dependence on N_o is straightforward and unsurprising; the greater the deep nitrogen concentrations, the greater the equilibrium value in the mixed layer is. The dependence on ($m_e + m_t$) and α is shown in Fig. 18, with all other values at their defaults for the biological model and a mixed layer depth of 30 m. At larger mixing rates concentrations approach the deep value ($N_o = 10$); as the vertical mixing decreases, the growth rate has a stronger effect on the equilibrium nitrogen concentration, with larger growth rates leading to lower nitrogen levels.

The equilibrium herbivore concentration is:

$$H^* = \phi P^* \gamma / c \quad (12)$$

Thus, the equilibrium herbivore concentration increases when their food source (P^*) or net grazing efficiency (ϕ) increases, and is proportional to the effective growth rate (γ). Note in particular that the equilibrium phytoplankton concentration is *not* dependent on the effective growth rate, while the equilibrium herbivore concentration is. In other words, increases in the growth rate translate to a larger herbivore population needed to eat the increased growth, while the phytoplankton population itself depends only on the efficiency of that grazing.

As outlined in EP85, disequilibrium conditions (and typically, a spring bloom) result when the specific rate of change of the equilibrium herbivore concentration, $(1/H^*)dH^*/dt$, is changing too rapidly to be tracked by the actual herbivore concentrations $(1/H)dH/dt$ (there is no issue with P^* changing too rapidly to be tracked since it is constant). From Eq. 12,

$$\frac{1}{H^*}\frac{dH^*}{dt} = \frac{1}{\gamma}\frac{d\gamma}{dt} \quad (13)$$

In particular, if γ increases through zero, the herbivore population is incapable of adjusting quickly enough to the altering environment, and a spring bloom generally results as the phytoplankton growth is unchecked by a sufficient herbivore population.

REFERENCES

Barnett, T. P., R. Malone, W. Pennell, D. Stammer, A. Semtner, W Washington, 2002: ACPI project overview and summary. *Climatic Change*.

Dukowicz, J. K., R. D. Smith, 1994: Implicit free-surface method for the Bryan-Cox-Semtner ocean model. *J. Geophys. Res.*, v. **99** p. 7991-8014.

Evans, G. T., J. S. Parslow, 1985: A model of annual plankton cycles. *Biological Oceanography*, v. **3** p. 327-347.

Frost, B. W., 1991: The role of grazing in nutrient-rich areas of the open sea. *Limnol. Oceanogr.*, v. **36** p. 1616-30.

Hunke, E. C., J. K. Dukowicz, 1997: An elastic-viscous-plastic model for sea ice dynamics. *J. Phys. Oceanogr.*, v. **27** p. 1849-67.

IPCC, , 2001: Climate Change 2001: Synthesis Report. Contribution of working groups I, II, and III to the third assessment report of the intergovernmental panel on climate change. Cambridge University Press, 397 pp.

Kiehl, J. T., J. J. Hack, G. B. Bonan, B. A. Boville, D. J. Williamson, P. J. Rasch, 1998: The National Center for Atmospheric Research Community Climate Model: CCM3. *J. Climate*, v. **11** p. 1131-1149.

Martin, J. H., R. M. Gordon, S. E. Fitzwater, 1990: Iron in Antarctic waters. *Nature*, v. **345** p. 156-8.

Mitchell, B. G., E. A. Brody, O. Holm-Hansen, C. McClain, J. Bishop, 1991: Light limitation of phytoplankton biomass and macronutrient utilization in the Southern Ocean. *Limnol. Oceanogr.*, v. **36** p. 1662-77.

Obata, A., J. Ishizaka, M. Endoh, 1996: Global verification of critical depth theory for phytoplankton bloom with climatological in situ temperature and satellite ocean color data. *J. Geophys. Res.*, v. **101** p. 20657-67.

Polovina, J. J., G. T. Mitchum, G. T. Evans, 1995: Decadal and basin-scale variation in mixed layer depth and the impact on biological production in the Central and North Pacific, 1960-88. *DSR*, v. **42** p. 1701-1716.

Sarmiento, J. L., R. D. Slater, M. J. Fasham, H. W. Ducklow, J. R. Toggweiler, G. T. Evans, 1993: A seasonal three-dimensional ecosystem model of nitrogen cycling in the North Atlantic euphotic zone. *Global Biogeochemical Cycles*, v. **7** p. 417-450.

Smith, R. D., J. K. Dukowicz, R. C. Malone, 1992: Parallel ocean general circulation modeling. *Physica D*, v. **60** p. 38-61.

Sverdrup, H. U., 1953: On conditions for the vernal blooming of phytoplankton. *J. Cons. Cons. Int. Explor. Mer*, v. **18** p. 287-295.

Washington, W. M., J. W. Weatherly, G. A. Meehl, A. J. Semtner, T. W. Bettge, A. P. Craig, W. G. Strand, J. Arblaster, V. B. Wayland, R. James, Y. Zhang, 2000: Parallel Climate Model (PCM) control and transient simulations. *Climate Dynamics*, v. **16** p. 755-74.

Zhang, J., W. D. Hibler, 1997: On an efficient numerical method for modeling sea ice dynamics. *J. Geophys. Res.*, v. **102** p. 8691-702.